6th International Conference on Climbing and Walking Robots

and the Support Technologies for Mobile Machines

Edited by
Giovanni Muscato
Domenico Longo

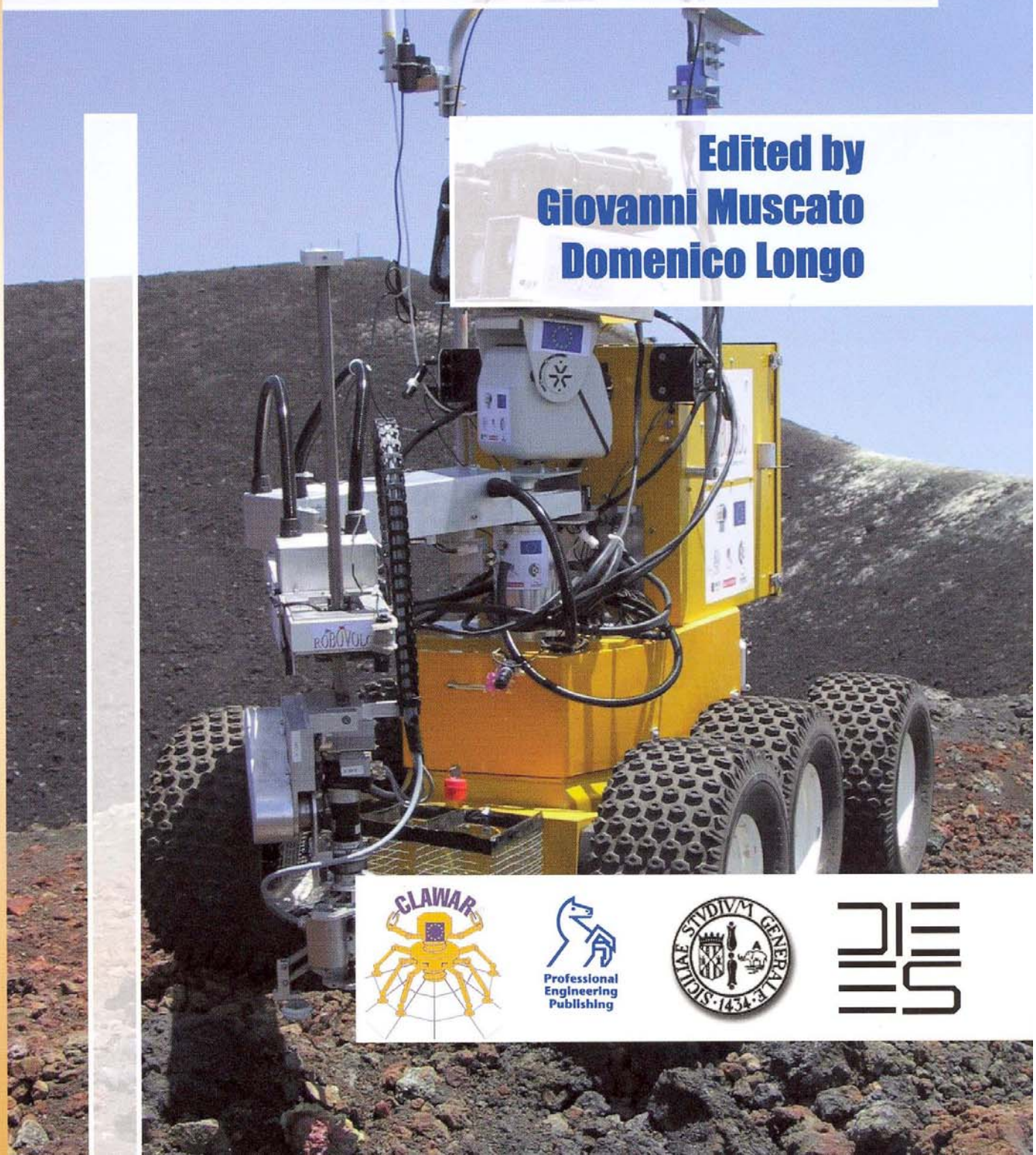

CLAWAR
Professional Engineering Publishing
STVDIVM GENERALE · SICILIAE · 1434 ·

Cascade control of a hexapod robot

M F SILVA and **J A TENREIRO MACHADO**
Department of Electrical Engineering, Institute of Engineering of Porto, Portugal
A MENDES LOPES
Department of Mechanical Engineering, Faculty of Engineering of Porto, Portugal

SYNOPSIS

This paper analyzes the performance of a hexapod robot under the action of a cascade controller involving position and force feedback loops. In order to evaluate the system properties we formulate several measures of the walking system based on the system dynamics and the trajectory errors. Simulation experiments reveal the influence of the different control algorithms upon the proposed indices.

1 INTRODUCTION

Walking machines allow locomotion in terrain inaccessible to other type of vehicles since they do not need a continuous support surface (1). On the other hand, the requirements for leg coordination and control impose difficulties beyond those encountered in wheeled robots (2). Previous studies addressed mainly the robot control, at the leg level, or the leg coordination, adopting strategies such as neural networks (3), fuzzy logic (4), hybrid force/position control (5), subsumption architecture (6) and insect-like schemes (7). In spite of the diversity of approaches, the control at the joint level is usually implemented through a simple PID algorithm with position/velocity feedback.

On a previous work were demonstrated the advantages of a cascade controller, with PD position control and foot force feedback, over a classical PD with, merely, position feedback (8). The present article presents a new algorithm that varies the gain in the forward force loop according with the step evolution. The aim is to analyze the performance of the controller through the viewpoint of several indices that measure, not only the system dynamics, but also the hip and foot trajectory errors during walking. The simulations reveal the superior performance of the controller with a gain adjusting scheme of the forward force loop during the support phase.

Bearing these facts in mind, the paper is organized as follows. Section two introduces the hexapod model and the motion planning scheme. Sections three and four present the robot control architecture and formulate the optimizing indices, respectively. Section five develops a set of experiments that reveal the performance of the different control algorithms. Finally, section six outlines the main conclusions and directions towards future developments.

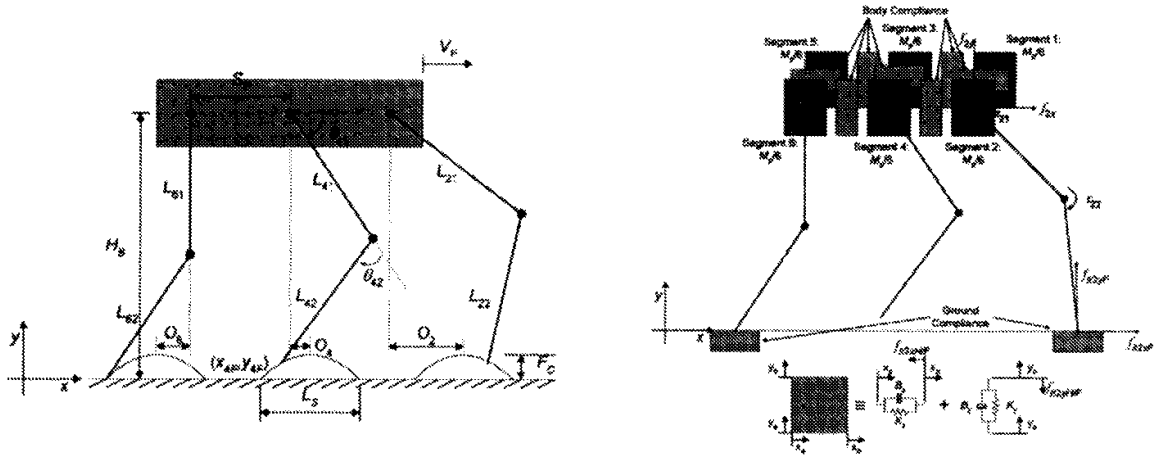

Fig. 1 Hexapod robot model
a) Coordinate system and variables b) Body and foot-ground dynamics

2 ROBOT KINEMATICS AND TRAJECTORY PLANNING

We consider a walking system with n legs, equally distributed along both sides of the robot body, having each one two rotational joints (Fig. 1a).

The kinematic model comprises: the cycle time T, the duty factor β, the transference time $t_T = (1-\beta)T$, the support time $t_S = \beta T$, the step length L_S, the stroke pitch S_P, the body height H_B, the maximum foot clearance F_C, the i^{th} leg lengths L_{i1} and L_{i2} and the foot trajectory offset O_i (i=1,...,n). Moreover, we consider a periodic trajectory for each foot, with body velocity $V_F = L_S T^{-1}$.

Given a particular gait and duty factor β, it is possible to calculate for leg i the corresponding phase ϕ_i and the time instant where each leg leaves and returns to contact with the ground (2). Knowing T, β and t_S, the cartesian trajectories of the tip of the foots must be completed during t_T. Based on this data, the trajectory generator is responsible for producing a motion that synchronises and coordinates the legs.

For each cycle the desired trajectory of the foot of the swing leg is computed either through a cycloid (Eq. 1a) or a sinusoidal (Eq. 1b) function. For example, considering that the transfer phase starts at t = 0 s for leg i = 1 we have for $\mathbf{p_{Fd}}(t) = [x_{iFd}(t), y_{iFd}(t)]^T$:

- during the transfer phase:

Cycloid function

$$\mathbf{p_{Fd}}(t) = \begin{bmatrix} V_F\left[t - \frac{1}{2\pi f}\sin\left(\frac{2\pi t}{T}\right)\right] \\ \frac{F_C}{2}\left[1-\cos\left(\frac{2\pi t}{T}\right)\right] \end{bmatrix}$$

Sinusoidal function

$$\mathbf{p_{Fd}}(t) = \begin{bmatrix} \left(\frac{t_T}{T}\right)\left[\left(\frac{L_S t}{t_T}\right) - \frac{L_S}{2\pi}\sin\left(\frac{2\pi t}{T}\right)\right] \\ \frac{2F_C t'}{T} - \frac{F_C}{2\pi}\sin\left(\frac{4\pi t'}{T}\right) \end{bmatrix}, \quad (1)$$

$$t' = \begin{cases} t, & 0 \le t < T/2 \\ T-t, & T/2 \le t < T \end{cases}$$

- during the stance phase:

$$\mathbf{p}_{\mathbf{Fd}}(t) = [V_F T \quad 0]^{\mathrm{T}} \tag{2}$$

The robot body is assumed to have a horizontal movement with a constant forward speed V_F. Therefore, for leg $i = 1$ the hip cartesian coordinates are given by $\mathbf{p_{Hd}}(t) = [x_{iHd}(t), y_{iHd}(t)]^{\mathrm{T}}$:

$$\mathbf{p}_{\mathbf{Hd}}(t) = [V_F t \quad H_B]^{\mathrm{T}} \tag{3}$$

Once defined the coordinates of the feet and hips of the robot it is possible to obtain the leg joint positions and velocities using the inverse kinematics ψ^{-1} and the Jacobian $\mathbf{J} = \partial\psi/\partial\boldsymbol{\theta}$.

The algorithm for the forward motion planning accepts the desired cartesian trajectories of the leg feet $\mathbf{p_{Fd}}(t)$ and hips $\mathbf{p_{Hd}}(t)$ as inputs and, by means of an inverse kinematics algorithm, generates the related joint trajectories $\boldsymbol{\theta}_{\mathbf{d}}(t) = [\theta_{i1d}(t), \theta_{i2d}(t)]^{\mathrm{T}}$, selecting the solution corresponding to a forward knee:

$$\begin{aligned}
&\mathbf{p}_{\mathbf{d}}(t) = \left[x_{id}(t) \quad y_{id}(t)\right]^{\mathrm{T}} = \mathbf{p}_{\mathbf{Hd}}(t) - \mathbf{p}_{\mathbf{Fd}}(t) \\
&\mathbf{p}_{\mathbf{d}}(t) = \psi\left[\boldsymbol{\theta}_{\mathbf{d}}(t)\right] \Rightarrow \boldsymbol{\theta}_{\mathbf{d}}(t) = \psi^{-1}\left[\mathbf{p}_{\mathbf{d}}(t)\right] \\
&\dot{\boldsymbol{\theta}}_{\mathbf{d}}(t) = \mathbf{J}^{-1}\left[\dot{\mathbf{p}}_{\mathbf{d}}(t)\right]
\end{aligned} \tag{4}$$

3 ROBOT DYNAMICS AND CONTROL ARCHITECTURE

The robot inverse dynamics is formulated as:

$$\boldsymbol{\tau} = \mathbf{H}(\boldsymbol{\theta})\ddot{\boldsymbol{\theta}} + \mathbf{c}\left(\boldsymbol{\theta}, \dot{\boldsymbol{\theta}}\right) + \mathbf{g}(\boldsymbol{\theta}) - \mathbf{J}^{\mathrm{T}}{}_{\mathbf{H}}(\boldsymbol{\theta})\mathbf{F}_{\mathbf{RH}} - \mathbf{J}^{\mathrm{T}}{}_{\mathbf{F}}(\boldsymbol{\theta})\mathbf{F}_{\mathbf{RF}} \tag{5}$$

where $\boldsymbol{\tau} = [f_{ix}, f_{iy}, \tau_{i1}, \tau_{i2}]^{\mathrm{T}}$ $(i=1,\ldots,n)$ is the vector of forces/torques, $\boldsymbol{\theta} = [x_{iH}, y_{iH}, \theta_{i1}, \theta_{i2}]^{\mathrm{T}}$ is the vector of position coordinates, $\mathbf{H}(\boldsymbol{\theta})$ is the inertia matrix and $\mathbf{c}\left(\boldsymbol{\theta}, \dot{\boldsymbol{\theta}}\right)$ and $\mathbf{g}(\boldsymbol{\theta})$ are the vectors of centrifugal/Coriolis and gravitational forces/torques, respectively. The $n \times m$ matrices $\mathbf{J}^{\mathrm{T}}{}_{\mathbf{H}}(\boldsymbol{\theta})$ and $\mathbf{J}^{\mathrm{T}}{}_{\mathbf{F}}(\boldsymbol{\theta})$ are the transposes of the robot Jacobian matrices, $\mathbf{F_{RH}}$ is the $m \times 1$ vector of the body inter-segment forces and $\mathbf{F_{RF}}$ is the $m \times 1$ vector of the reaction forces that the ground exerts on the robot feet. It is considered that these forces are null during the foot transfer phase. Furthermore, we consider that the joint actuators are not ideal, exhibiting a saturation given by:

$$\tau_{mij} = \begin{cases} \tau_{Cij} & , \left|\tau_{mij}\right| \le \tau_{Max} \\ \mathrm{sgn}\left(\tau_{Cij}\right) \cdot \tau_{Max} & , \left|\tau_{mij}\right| > \tau_{Max} \end{cases} \tag{6}$$

where, for leg i and joint j, τ_{Cij} is the controller demanded torque, τ_{Max} is the maximum torque that the actuator can supply and τ_{mij} is the motor effective torque.

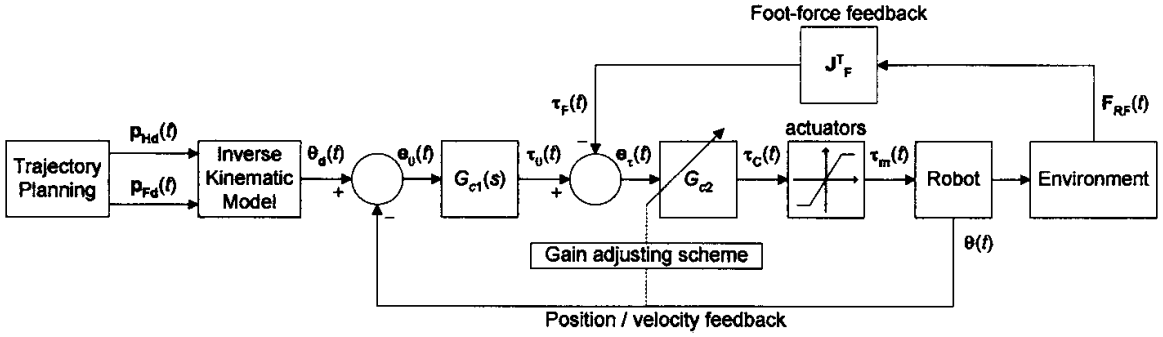

Fig. 2 Hexapod robot control architecture

Figure 1b presents the dynamic model for the hexapod body and foot-ground interaction. The contact of the i^{th} robot feet with the ground is modeled through a linear system with damping $B_{i\eta}$ and stiffness $K_{i\eta}$ ($\eta = \{x, y\}$) in the {horizontal, vertical} directions, respectively. The same type of model is adopted to implement the compliance between the n segments of the robot body. Therefore, we divide the robot body in n identical segments, each segment (with mass $M_b n^{-1}$) corresponding to a robot hip connected to the neighbour segments through a spring-dashpot model.

The control architecture of the hexapod robot is presented in Fig. 2. For $G_{c1}(s)$ we adopt a position/velocity *PD* algorithm:

$$G_{C1_j}(s) = Kp_j + Kd_j s \quad , j = 1,2 \tag{7}$$

where Kp_j and Kd_j are the proportional and derivative gains. For G_{c2} we consider a simple *P* controller with gain Kp_j that is varied according to a scheme described in the sequel.

In order to tune the controller we adopt a "brute-force" method, testing and evaluating several possible combinations of parameters. Since the essence of locomotion is to move smoothly the section of the upper body from one place to another, with some restrictions in terms of execution time, we select, for each case, the set of parameters that minimise the mean square errors of the robot hip trajectory (Eq. 12) during one complete step.

4 MEASURES FOR PERFORMANCE EVALUATION

We establish several distinct measures of the mechanism performance in an average sense. In this perspective, we define four indices $\{E_{av}, T_L, F_L, \tau_P\}$ inspired on the robot dynamics and four indices $\{\varepsilon_{xH}, \varepsilon_{yH}, \varepsilon_{xF}, \varepsilon_{yF}\}$ based on the trajectory tracking errors.

A first measure in this analysis is the mean absolute density of energy per travelled distance. This index is computed assuming that energy regeneration is not available by actuators doing negative work (by taking the absolute value of the power). Consequently, the index E_{av} is obtained by averaging the mechanical absolute energy delivered over the travelled distance L:

$$E_{av} = \frac{1}{L}\sum_{i=1}^{n}\sum_{j=1}^{m}\int_0^T \left|\tau_{ij}(t)\dot{\theta}_{ij}(t)\right| dt \tag{8}$$

A second index consists on T_L, the density of power lost in the joint actuators per travelled distance L, that is:

$$T_L = \frac{1}{L}\sqrt{\sum_{i=1}^{n}\sum_{j=1}^{m}\int_0^T \left[\tau_{ij}(t)\right]^2 dt} \tag{9}$$

A third measure is the index F_L that considers the forces that occur on the hips of the robot per travelled distance L:

$$F_L = \frac{1}{L}\sqrt{\sum_{i=1}^{n}\sum_{j=1}^{m}\int_0^T \left\{\left[f_{ix}(t)\right]^2 + \left[f_{iy}(t)\right]^2\right\} dt} \tag{10}$$

Since the previous indices capture, mainly, the low frequency system behaviour we define the index τ_P that measures the robot torque peaks demanded by the controller when responding to high frequency phenomena, such as foot-ground impacts:

$$\tau_P = \max\left|\tau_{Cij}(t)\right| \tag{11}$$

In what concerns the hip and foot trajectory following errors we can define the indices:

$$\varepsilon_{\eta\mu} = \sum_{i=1}^{n}\sqrt{\frac{1}{N_S}\sum_{k=1}^{N_S}\Delta_{i\eta\mu}{}^2}, \quad \Delta_{i\eta\mu} = \eta_\mu^d(k) - \eta_\mu^r(k), \quad \eta = \{x, y\}, \quad \mu = \{H, F\} \tag{12}$$

where N_S is the total number of samples for averaging purposes, $\{d, r\}$ indicate the i^{th} samples of the desired and real position and the subscripts $\eta = \{x, y\}$ and $\mu = \{H, F\}$ represent the {horizontal, vertical} and the {hip, foot} coordinates, respectively.

In all cases the performance optimization requires the minimization of each index.

5 SIMULATION RESULTS

In this section we compare the controller performances during a periodic wave gait. Consequently, we consider the parameters $\beta = 50\%$, $L_S = 1$ m, $H_B = 0.9$ m, $F_C = 0.1$ m, $V_F = 1$ ms^{-1}, $S_P = 1$ m, $L_{i1} = L_{i2} = 0.5$ m, $O_i = 0$ m, $M_{i1} = M_{i2} = 1$ kg, $M_b = 88.0$ kg and $M_{if} = 0$ kg. The robot body is modelled with $K_{ix} = 10^5$ Nm^{-1}, $K_{iy} = 10^4$ Nm^{-1}, $B_{ix} = 10^3$ Nsm^{-1} and $B_{iy} = 10^2$ Nsm^{-1}. Furthermore, the ground properties are characterised by $K_{ix} = 10^5$ Nm^{-1}, $K_{iy} = 10^6$ Nm^{-1}, $B_{ix} = 10^3$ Nsm^{-1} and $B_{iy} = 10^4$ Nsm^{-1}.

The controllers are tuned assuming high performance robot actuators with a maximum actuator torque in (6) of $\tau_{Max} = 400$ Nm. The minimisation of the hips and feet trajectories errors, leads to the $G_{c1}(s)$ controller parameters Kp_j =2000 and Kd_j = 50 and a proportional controller G_{c2} with gain $Kp_j = 0.9$ ($j = 1, 2$).

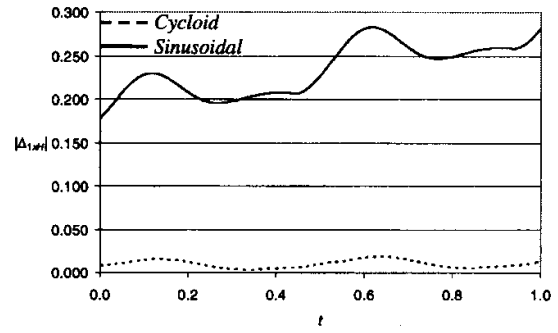

Fig. 3 Plots of the hip trajectory error $|\Delta_{1xH}|$ *vs.* t for the *cycloid* and *sinusoidal* feet trajectories

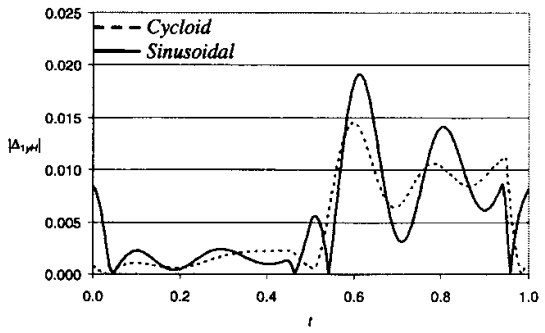

Fig. 4 Plots of the hip trajectory error $|\Delta_{1yH}|$ *vs.* t for the *cycloid* and *sinusoidal* feet trajectories

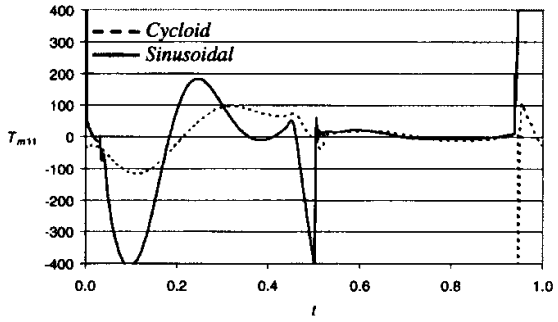

Fig. 5 Plots of the joint torque T_{m11} *vs.* t for the *cycloid* and *sinusoidal* feet trajectories

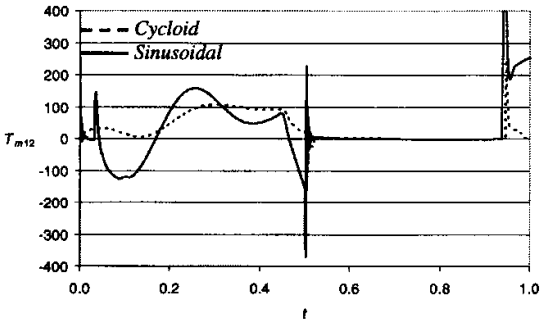

Fig. 6 Plots of the joint torque T_{m12} *vs.* t for the *cycloid* and *sinusoidal* feet trajectories

For this set of robot, ground and controller parameters we evaluated the two alternative foot trajectories (Eq. 1). From figures 3 – 6 it is possible to conclude that the cycloid is superior to the sinusoidal function because improves the hip and foot trajectory tracking, while minimising the corresponding joint torques. For different acceleration profiles of the foot trajectory there were no significant changes of these charts. Based on this conclusion, we adopt the cycloidal foot trajectory while testing the controller performances for distinct strategies in the G_{c2} gain definition.

Figures 7 – 8 reveal that increasing the proportional gain Kp_j, in the controller G_{c2}, leads to a better trajectory following of the robot hips and feet trajectories but, on the other hand, degrade the dynamical indices (Figs. 9 – 10). Moreover, high gains lead to large feet-ground impacts that propagate through the control loop up to the actuators, as can be seen in Figs. 11 – 12.

Bearing these facts in mind we can establish a gain scheduling policy that varies the gain in accordance with the feet relative position to the ground. Therefore, a scheme $Kp_j(y_{iF}) = Kp_{jlow}$ if $y_{iF} \leq y_{iF0}$ or $Kp_j(y_{iF}) = Kp_{jhigh}$ if $y_{iF} > y_{iF0}$ for $\{Kp_{jlow}, Kp_{jhigh}, y_{iF0}\} = \{0.4, 0.9, 0.01\}$ leads to a good compromise between the trajectory following errors and the dynamic indices, as can be seen in Figs. 13 – 14.

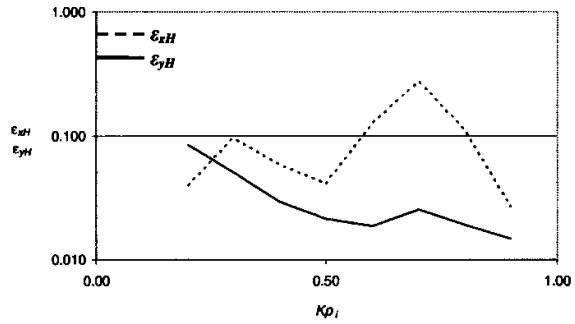

Fig. 7 Plots of ε_{xH} and ε_{yH} *vs.* Kp_{jlow}, with $\{Kp_{jhigh}, y_{iF0}\} = \{0.9, 0.01\}$

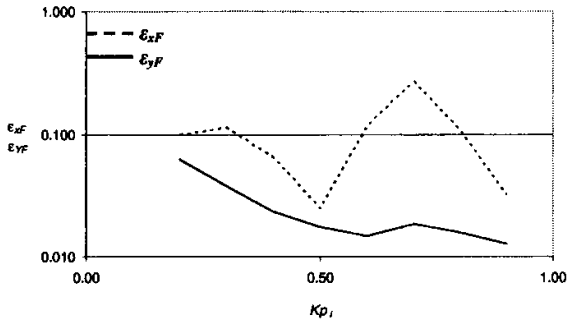

Fig. 8 Plots of ε_{xF} and ε_{yF} *vs.* Kp_{jlow}, with $\{Kp_{jhigh}, y_{iF0}\} = \{0.9, 0.01\}$

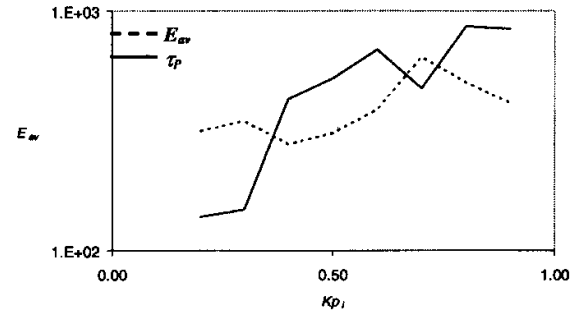

Fig. 9 Plots of E_{av} and τ_P *vs.* Kp_{jlow}, with $\{Kp_{jhigh}, y_{iF0}\} = \{0.9, 0.01\}$

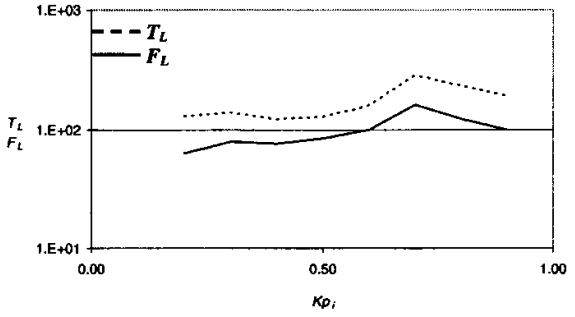

Fig. 10 Plots of F_L and T_L *vs.* Kp_{jlow}, with $\{Kp_{jhigh}, y_{iF0}\} = \{0.9, 0.01\}$

In conclusion, the foot-force feedback with a reduction of the proportional gains of the forward loop during the support phase seems essential for establishing a robust control during walking and to accommodate foot-ground interaction phenomena.

6 CONCLUSIONS

In this paper we have studied the performance of a cascade controller involving position and force feedback loops, in hexapod robots.

For analyzing the system performance several quantitative measures were defined based on the system dynamics and the hip and foot trajectory errors. The experiments reveal that a cascade controller with the foot-force feedback and a reduction of the proportional gains of the forward force loop during the support phase seems superior, from the point of view of the proposed indices.

While our focus has been on a dynamic analysis in periodic gaits many aspects of locomotion are not necessarily captured by the proposed measures. Consequently, future work in this area will address the refinement of our models to incorporate other characteristics of the robot actuators and the joint transmissions. Further studies are also being developed in order to design superior control architectures that include more sophisticated algorithms.

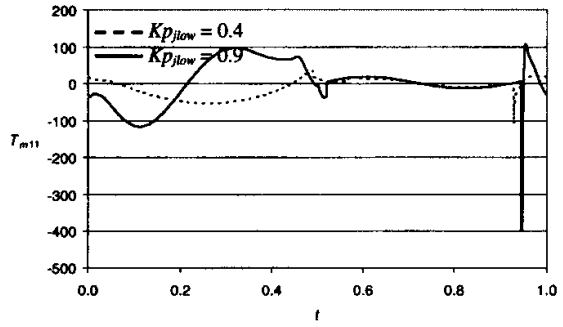

Fig. 11 Plots of the joint torque T_{m11} *vs.* t, with $\{Kp_{jlow}, Kp_{jhigh}, y_{iF0}\} = \{0.4, 0.9, 0.01\}$

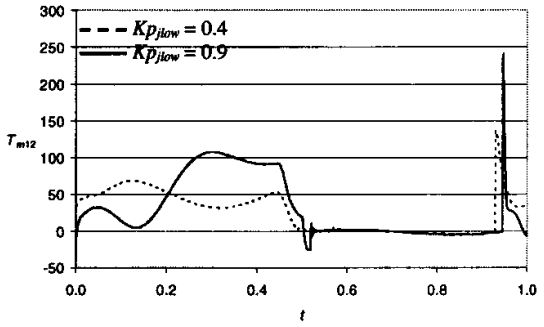

Fig. 12 Plots of the joint torque T_{m12} *vs.* t, with $\{Kp_{jlow}, Kp_{jhigh}, y_{iF0}\} = \{0.4, 0.9, 0.01\}$

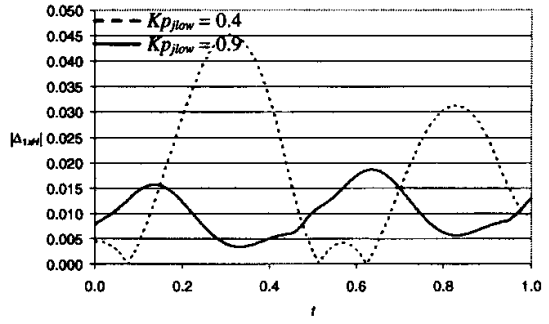

Fig. 13 Plots of the hip trajectory error $|\Delta_{1xH}|$ *vs.* t, with $\{Kp_{jlow}, Kp_{jhigh}, y_{iF0}\} = \{0.4, 0.9, 0.01\}$

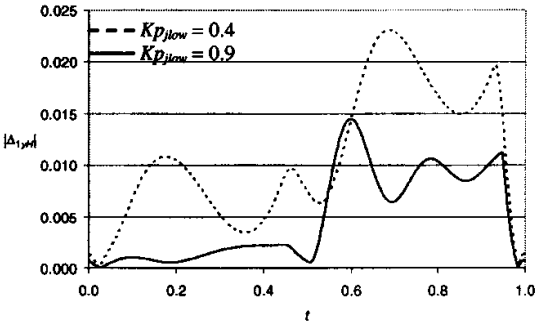

Fig. 14 Plots of the hip trajectory error $|\Delta_{1yH}|$ *vs.* t, with $\{Kp_{jlow}, Kp_{jhigh}, y_{iF0}\} = \{0.4, 0.9, 0.01\}$

REFERENCES

1 **Manko, D. J.** A General Model of Legged Locomotion on Natural Terrain. Kluwer. Westinghouse Electric Corporation. 1992.

2 **Song, S.-M.** and **Waldron, K.J.** Machines that Walk: The Adaptive Suspension Vehicle. The MIT Press. 1989.

3 **Tsai, C.-R.** and **Lee, T.-T.** (1998) A Study of Fuzzy-Neural Force Control for a Quadrupedal Walking Machine. In *Journal of Dynamic Systems, Measurement and Control*, **120**, pp. 124 – 133.

4 **Tsai, C.-R., Lee, T.-T. and Song, S.-M.** (1997) Fuzzy Logic Control of a Planetary Gear Type Walking Machine Leg. In *Robotica*, 15, pp. 533 – 546.

5 **Song, J. , Low K. H.** and **Guo, W.** (1999) A Simplified Hybrid Force/Position Controller Method for the Walking Robots. In *Robotica*, **17**, pp. 583 – 589.

6 **Brooks, R. A.** (1989) A Robot That Walks; Emergent Behaviours From a Carefully Evolved Network. *A.I. Memo 1091*, Artificial Intelligence Laboratory, MIT.

7 **Ferrell, C.** (1995) A Comparison of Three Insect Inspired Locomotion Controllers. In *Robotics and Autonomous Systems*. **16**, pp. 135 – 159.

8 **Silva, M. F.** and **Machado, J. A. T.** (2003) Position and Force Control of a Walking Hexapod. ICAR'03 – 11th Int. Conf. on Advanced Robotics, Portugal, pp. 1743 – 1748.